






Article

Biomass Fly Ash Self-Hardened Adsorbent Monoliths for Methylene Blue Removal from Aqueous Solutions

Marinélia N. Capela ^{1,*}, Francielly R. Cesconeto ¹, Paula C. Pinto ², Luís A. C. Tarelho ³, Maria P. Seabra ^{1,*}
and João A. Labrincha ¹

- ¹ Department of Materials and Ceramic Engineering, CICECO-Aveiro Institute of Materials, University of Aveiro, 3810-193 Aveiro, Portugal; franciellycesconeto@gmail.com (F.R.C.); jal@ua.pt (J.A.L.)
² RAIZ-Forest and Paper Research Institute, Quinta de São Francisco, 3800-783 Aveiro, Portugal; paula.pinto@thenavigatorcompany.com
³ Department of Environment and Planning, CESAM-Centre for Environmental and Marine Studies, University of Aveiro, 3810-193 Aveiro, Portugal; ltarelho@ua.pt
* Correspondence: marinelia.capela@ua.pt (M.N.C.); pseabra@ua.pt (M.P.S.)

Featured Application: Development of inexpensive waste-based porous bulk adsorbents with methylene blue adsorption capacity.

Abstract: The use of methylene blue (MB) by several industries generates contaminated industrial wastewaters that must be purified before discharge into the environment. Its removal can be achieved by adsorption, and low-cost and easily available materials should be used as adsorbents. Biomass fly ash (BFA) generated from biomass combustion, for heat and power generation, is increasing worldwide since the process is considered CO₂ neutral. However, most of the ash is still landfilled. This study aims to evaluate the valorisation of BFA as a low-cost porous bulk adsorbent for MB removal from wastewaters. The monoliths were obtained after 14 days of curing just after adding water and a porogenic agent (aluminium powder) to the BFA, using the self-hardening ability of this waste. The BFA was characterised for chemical (XRF) and mineralogical (XRD) composition, particle size distribution (laser diffraction-COULTER) and morphology (SEM). The monolith sample cured for 14 days was characterised for density, porosity (total and open), microstructure, compressive strength, and MB removal ability (batch tests). The results showed that the addition of aluminium powder (0.09 wt.%) promoted an increase in interconnected porosity and the MB removal efficiency reached 80% for the most porous samples. The equilibrium data for the adsorption process were well characterised by a type 2 Langmuir isotherm equation with a monolayer adsorption capacity (q_{max}) that ranged from 0.22 to 0.66 mg/g.

Keywords: biomass fly ash; self-hardening; green processing; bulk porous adsorbents; dye removal; micropollutants; sorption



Citation: Capela, M.N.; Cesconeto, F.R.; Pinto, P.C.; Tarelho, L.A.C.; Seabra, M.P.; Labrincha, J.A. Biomass Fly Ash Self-Hardened Adsorbent Monoliths for Methylene Blue Removal from Aqueous Solutions. *Appl. Sci.* **2022**, *12*, 5134. <https://doi.org/10.3390/app12105134>

Academic Editor: Dragana Mutavdžić Pavlović

Received: 2 May 2022

Accepted: 18 May 2022

Published: 19 May 2022

Publisher's Note: MDPI stays neutral with regard to jurisdictional claims in published maps and institutional affiliations.



Copyright: © 2022 by the authors. Licensee MDPI, Basel, Switzerland. This article is an open access article distributed under the terms and conditions of the Creative Commons Attribution (CC BY) license (<https://creativecommons.org/licenses/by/4.0/>).

1. Introduction

Global water demand for irrigation, domestic use, manufacturing, livestock, and electricity is expected to increase by 55% between 2000 and 2050 (3500 km³ in 2000 for approximately 5500 km³ by 2050) [1]. To avoid water shortage, the proper treatment of wastewater is of utmost importance [1] since it may provide a source of clean water and soften the water scarcity [2].

The use of dyes in industries such as textile, leather, paper and plastics generates considerable amounts of tinted wastewater [3]. In the textile industry, methylene blue (MB) is the most-used dye to colour cotton, wood, and silk [3]. Yet, MB may cause damaging consequences to human health, such as blindness, respiratory distress and abdominal disorders. Therefore, its removal from wastewaters is extremely important [3,4].

Adsorption is considered the most effective and simple method of water decontamination [2,3]. It has a low cost, simple layout, easy operation and insensitivity to toxic pollutants [3]. Due to this, the number of published research works on MB removal from wastewater is very significant (5545 for “adsorbents and methylene blue”, data obtained from the Scopus database in December 2021). However, the development of environmentally friendly low-cost adsorbent materials remains a challenge.

Nowadays, the combustion of biomass is a relevant alternative technology to generate useful energy (heat and power) since it is considered carbon-neutral [5–7]. Nonetheless, this process produces huge quantities of biomass ash (BA). In 2018, it was estimated that nearly 10 million tonnes of BA were generated worldwide only for power production [8]. The amount is certainly much higher nowadays since new conversion plants were built due to the implementation of decarbonisation policies, such as the European Union’s low-carbon economy roadmap [9]. The proper management of the produced ashes is essential for the sustainability of the biomass to energy practice [10]. One of the most used biomass combustion technologies for heat and power production is bubbling fluidised bed combustion (BFBC). BFBC generates two ash fluxes: biomass fly ash (BFA) that is collected in the super-heaters, economisers and air pollution control devices (cyclones, bag-filters, electrostatic precipitators); and, bottom bed ash (BBA), usually coarser in size, resulting from periodic discharges of the sand bed mixed with BA [10]. Both BFA and BBA are composed of particles from the original sand bed, inorganic content of the biomass, exogenous inorganic materials (soil and small stones) attached to biomass and unburnt fuel [10]. Commonly, these two streams of ash are landfilled [10], so their recycling is important from environmental and economic viewpoints.

One innovative and environmentally friendly application for BFA is its use as a raw material for the production of bulk adsorbents, exploiting its self-hardening ability. BFA, when mixed with water, can harden [5–7] and form monoliths with enough mechanical strength for some applications. The adsorption capacity of the samples can be enhanced by increasing their porosity using a foaming agent, such as aluminium powder (AP). A dense structure limits the permeability to liquids, so the existence of interconnected pores will favour the adsorption performance. The use of bulk adsorbents represents an improvement on the use of BFA by itself because it will allow their direct utilisation in packed beds (powdered adsorbents may need to be used inside a container [2]) and, after use, they can be easily collected [4].

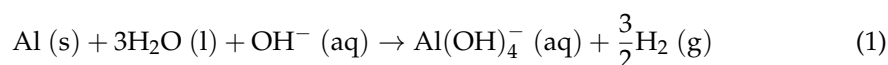
In this work, and for the first time, low-cost BFA self-hardened bulk adsorbents with controlled porosity were produced. Their performance as MB adsorbents from aqueous solutions was evaluated in batch tests. A commercial Portland limestone cement (PLC) was added to prevent porous coalescence by accelerating the hardening process. PLC also enhances material strength, especially at an early age. The effect of AP and PLC contents on the hardened-state properties (compressive strength, density, microstructure, total and open porosity) of the ash-based monoliths was evaluated. MB’s initial concentration and contact time were the parameters evaluated in adsorption trials.

2. Materials and Methods

2.1. Materials

Biomass fly ash (BFA) was collected along three consecutive production days at a biomass cogeneration plant, operating in a pulp and paper mill, equipped with a bubbling fluidised bed boiler (BFBB) with an installed power of 99 MW. The combustion temperature is around 825 °C and sand is used as the bottom bed. Eucalyptus bark and small amounts of knots, which are organic rejects produced from the pulp screening process, were used as fuel. A batch composed of equal amounts of the samples collected each day was prepared, then dried in a ventilated laboratory oven at 105 °C and sieved through a 2 mm mesh (Retsch AS200, Haan, Germany). Afterwards, the BFA was kept in closed opaque polypropylene containers before characterization and monoliths production.

A commercial aluminium powder (AP) (Expandit BE 1101, Grimm Metallpulver GmbH, Roth, Germany) was employed as a porogenic agent. In an alkaline medium, the AP reacts with water, releasing gaseous hydrogen following the Chemical reaction (1) [11]:



The formation of H₂ bubbles during the mixing and self-hardening processes generates pores. To stabilise the foam, a commercial surfactant (Hotaspor OSB, Clariant, Barcelona, Spain) was used. A commercial Portland limestone cement (PLC) (type II/B-L 32.5 N) was also used aiming to preserve the formed porous structure, by accelerating the hardening process while improving the mechanical strength of the cured monoliths.

Methylene blue (MB), a cationic dye (C₁₆H₁₈ClN₃S, Sigma Aldrich, Steinheim, Germany) was selected to evaluate the monoliths' adsorption capacity due to its stability in alkaline environments, as well as its widespread use in several industries [12].

2.2. Preparation of the Self-Hardened Monoliths

BFA-based slurries, without and with 5 wt.% of PLC (by replacing the weight of the BFA), were prepared. They contain 0.05 wt.% (of the total solid content) of surfactant and distinct amounts of AP (0.00, 0.01, 0.05 and 0.09 wt.% of the total solids content). The use of the same surfactant concentration in all the prepared slurries was established because this type of compound interferes with the adsorption process [13]. A water to total solids weight ratio (w/s) of 0.42 was used to prepare the slurries, assuring an adequate consistency for pouring and filling the moulds. The sample notation used here based on its composition is xC:yA, xC for PLC and yA for AP percentages. For example, the 5C:9A slurry has 5 wt.% of PLC and 0.09 wt.% of AP.

The prepared compositions are presented in Table 1.

Table 1. Composition of the monoliths.

Slurries	Raw Materials (g)				
	Water	BFA	PLC	AP	Surfactant
0C:0A	42	100	0	0.00	0.00
0C:1A	42	100	0	0.01	0.05
0C:5A	42	100	0	0.05	0.05
0C:9A	42	100	0	0.09	0.05
5C:0A	42	95	5	0.00	0.00
5C:1A	42	95	5	0.01	0.05
5C:5A	42	95	5	0.05	0.05
5C:9A	42	95	5	0.09	0.05

Single BFA or BFA/PLC blended powders were mixed in a plastic bag and then added to tap water in a mechanical mixer (KitchenAid, Artisan 175PS, Benton Harbor, MI, USA). Mixing for 2 min at a low rotation speed (60 rpm) was conducted. The mixer was stopped for 1 min to remove the material stuck to the edges of the bowl and place it again in the centre and mixed again for 8 min at the same rotation speed (60 rpm). Then, the AP and the surfactant were added, and the mixer was turned on for another 2 min at 60 rpm. The formation of H₂ starts after the addition of AP to the blends and continues for some minutes. The slurries were then poured into cubical silicone moulds (2.5 × 2.5 × 2.5 cm³), that were previously swabbed with olive oil. Afterwards, the moulds were placed in a sealed container with water at the bottom (>95% relative humidity) and cured for 7 days at ambient temperature (22 ± 2 °C). Then, the moulds were placed in a laboratory oven at 50 °C for 5 days. The samples were removed from the mould and kept in the oven at the same temperature for 2 more days. The curing conditions were chosen following the experimental procedure described by Illikainen et al. [5] and Ohenoja et al. [6,7].

2.3. Raw Materials and Self-Hardened Monoliths Characterization

The chemical composition of BFA and PLC was determined by X-ray fluorescence (XRF) (Philips X'Pert PRO MPD spectrometer, Almelo, The Netherlands) on a compressed powder pellet (10 g of sample was homogenised with five drops of polyvinyl alcohol and pressed to a standardised shape). The loss on ignition (LOI) at 1000 °C (15 min dwell time) was also determined. The specific surface area was measured by physical nitrogen adsorption isotherms using the Brunauer, Emmett, and Teller (BET) method (Micromeritics, Gemini 2370 V5.00, Norcross, GA, USA). The particle size distribution was obtained by the laser diffraction technique (Beckman Coulter LS 230 FM, Brea, CA, USA) employing the Fraunhofer model and the wet (water) procedure. The true density was determined by the helium pycnometer technique (Anton Paar GmbH, Ultrapyc 3000, Graz, Austria).

The mineralogical composition of BFA and self-hardened samples was evaluated by X-ray powder diffraction (XRD) at room temperature. The XRD was conducted on a θ/θ diffractometer (Malvern, PANalytical, X'Pert Pro3, Almelo, The Netherlands), equipped with a fast RTMS detector (Malvern PANalytical, PIXcel 1D, Almelo, The Netherlands), with Cu K α radiation (45 kV and 40 mA, 10–80° 2 θ range, with a virtual step scan of 0.026° 2 θ range, and virtual time per step of 100 s). For this analysis, the samples were grounded in an agate mortar until the whole sample passed through a 63 μ m sieve.

The morphology of BFA, PLC and AP powders, and the microstructure of the prepared monoliths cured for 14 days were accessed by scanning electron microscopy (SEM) (Hitachi, SU-70, Tokyo, Japan). Before SEM examination, the samples were coated with a carbon thin film (Emitech, K950, Fall River, MA, USA) to provide a conducting layer. The microstructure of the monoliths cured for 14 days was also observed in an optical microscope (Leica EZ4HD, Wetzlar, Germany).

For each composition, three cubical samples (14 days curing) were used for uniaxial compressive strength determination. The tests were performed, at room temperature, in a Universal Testing Machine (Shimadzu, model AG-25 TA refresh, Kyoto, Japan; provided with a 250 kN load cell running at a displacement rate of 0.5 mm/min). The density of the monoliths was obtained by measuring their mass and dimensional volume.

Monoliths total porosity (x_t) was measured by the Archimedes method, taking the weight of the samples in the dry (wt_1) and wet (wt_2) conditions and immersed in water (wt_3), following the Equation (2):

$$x_t = 1 - \frac{\rho_w}{\rho_{th}} \times \frac{wt_1}{wt_2 - wt_3} \quad (2)$$

where ρ_w is the density of liquid water at atmospheric conditions of pressure and temperature, and ρ_{th} is the true density of the hardened samples determined by the helium pycnometer technique. The reported values are the average of three measurements. Open porosity (x_0) was also calculated by the Equation (3):

$$x_0 = \frac{wt_2 - wt_1}{wt_2 - wt_3} \quad (3)$$

2.4. MB Adsorption Experiments

An MB stock solution, with a concentration of 1000 ppm, was prepared by dissolving an appropriate quantity of MB in 1 L of deionised water. MB solutions with 1, 2.5, 5, 10, and 15 ppm (initial concentration, C_0) were obtained by stock solution dilution with deionised water. To prevent photodegradation of the dye, all containers of the solutions were wrapped with aluminium foil and stored in the dark.

The cubic monoliths were sliced (Struers Secotom-10, Cleveland, OH, USA) in smaller parallelepiped ($0.5 \times 1.5 \times 2.0$ mm³) samples that were used in the MB adsorption tests. Their weight, which depends on the porosity of the samples, was between 0.752 g and 1.638 g. The MB adsorption was tested by immersing each monolith in glass beakers with 100 mL of MB solutions, at room temperature (22 ± 2 °C), under constant magnetic

stirring for a predetermined period (25 h). All adsorption experiments were performed at a pH value of around 6.5.

The MB concentration was determined through the absorption intensity at 664 nm (the main absorption band of MB) by UV spectroscopy (Shimadzu UV-3100, Kyoto, Japan). For that, aliquots of 1 mL were collected from the solution, at predefined time intervals (0–25 h). Two replicas were used, and the average value was presented. The conversion of the absorbance values into MB concentration was carried out using a calibration curve previously obtained from solutions of known concentration also obtained by stock solution dilution. The pH value during the experiments was measured (Thermo Fisher Scientific, Orion Star™ A211, Waltham, MA, USA). The tested variables were the contact time and MB initial concentration.

2.4.1. MB Uptake and Removal Efficiency

The quantity of adsorbed dye (q_e) was calculated using the Equation (4) [2,4,12,14]:

$$q_e = \frac{(C_0 - C_f)}{m} \times V \quad (4)$$

where: q_e is the amount of MB adsorbed by the monolith (mg MB/g monolith), C_0 is the initial concentration of the MB aqueous solution (ppm), C_f is the MB concentration (ppm) after the adsorption test, V is the solution volume (L) and m is the mass of the monolith (g).

The removal efficiency (E) was calculated by using the Equation (5) [2,4,12,14]:

$$E (\%) = \frac{(C_0 - C_f)}{C_0} \times 100 \quad (5)$$

2.4.2. Isotherm Models

Langmuir and Freundlich's adsorption isotherm models have been tested, by fitting the experimental results, to describe the adsorption mechanism.

The Langmuir isotherm model (Equation (6)) [2,4,12,14] assumes that homogeneous sorption occurs at the active sites of the sorbent and that the process ends once these sites are all filled, as there is no interaction between the adsorbed species (formation of a monolayer):

$$q_e = \frac{K_L \times q_{max} \times C_f}{1 + K_L \times C_f} \quad (6)$$

where K_L (L/mg) is the affinity of the sorbate for the binding sites and q_{max} (mg/g) is the maximum adsorption capacity. After achieving the K_L value, the Langmuir isotherm can be expressed by a separation factor, R_L , given by Equation (7) [2,4,12,14]:

$$R_L = \frac{1}{1 + K_L \times C_0} \quad (7)$$

If R_L is between 0 and 1 the adsorption is favourable, if >1 is unfavourable: if it is equal to 1 it is linear and if it is 0 it is irreversible [15].

Freundlich isotherm model (Equation (8)) assumes that the surface has sites with different affinities so the adsorption is not homogeneous [2,4,12].

$$q_e = K_F C_f^{\frac{1}{n}} \quad (8)$$

where: K_F is the Freundlich constant, n is a constant which represents the absence of linearity of the adsorbed quantity in the function of C_f . If n is between 1 and 10 the adsorption is favourable.

2.4.3. Adsorption Kinetics

To describe the adsorption kinetics of MB by the samples the pseudo-first-order and pseudo-second-order kinetic models were evaluated.

The pseudo-first-order kinetic model is given by Equation (9) [16]:

$$\log(q_e - q_t) = \log q_e - \frac{K_1 t}{2.303} \quad (9)$$

where: q_e is the adsorption capacity at equilibrium (mg/g), q_t (mg/g) is the amount of MB adsorbed at the time t (min), and K_1 is the rate constant of pseudo-first-order adsorption (1/min).

The pseudo-second-order kinetic model is expressed by Equation (10) [16–18]:

$$\frac{t}{q_t} = \frac{1}{K_2 q_e^2} + \frac{t}{q_e} \quad (10)$$

where: q_e is the adsorption capacity at equilibrium (mg/g), q_t (mg/g) is the adsorption capacity at time t (min), and K_2 is the pseudo-second-order rate constant (g/mg min).

3. Results and Discussion

3.1. Raw Materials Characterization

The chemical composition of BFA and PLC, expressed in terms of oxides, is shown in Table 2. The main components of BFA are CaO (32.3 wt.%), SiO₂ (21.8 wt.%), K₂O (9.28 wt.%) and Al₂O₃ (8.74 wt.%), which are in accordance with the results reported by other authors [10,19,20]. However, the characteristics of BFA may vary with the properties of the biomass used as fuel and the operating conditions [10]. In the case of PLC, the five main constituents are CaO (73.1 wt.%), SiO₂ (13.0 wt.), SO₃ (4.02 wt.%), Fe₂O₃ (2.94 wt.%) and Al₂O₃ (2.78 wt.%) which are in the usual concentrations reported for commercial PLC [19]. BFA has an LOI value of 10.48 wt.%.

Table 2. Chemical composition and LOI of BFA and PLC.

Compounds (wt.%)	BFA	PLC
CaO	32.3	73.1
SiO ₂	21.8	13.0
K ₂ O	9.28	1.69
Al ₂ O ₃	8.74	2.78
Cl	6.21	0.13
Na ₂ O	6.04	0.35
MgO	4.40	1.53
Fe ₂ O ₃	4.40	2.94
SO ₃	3.74	4.02
P ₂ O ₅	1.30	0.18
MnO	0.91	0.04
TiO ₂	0.55	0.16
CaO/SiO ₂	1.48	5.62
(CaO + MgO)/SiO ₂	1.68	5.74
LOI	10.48	16.41

The chemical composition of the ash, namely the CaO content, is extremely important for its potential self-hardening. According to EN197-1:2011 [21], a hydraulic binder is defined as a material that, when mixed with water, sets and hardens, and can maintain its strength and stability even while submerged in water. In the same standard, it is also mentioned that for Portland cement clinker to be considered a hydraulic material, the CaO/SiO₂ ratio (by mass) should be higher than 2, while a granulated blast furnace slag possesses hydraulic properties when the (CaO + MgO)/SiO₂ ratio (by mass) surpasses 1.0. The actual BFA only complies with the last requirement (see Table 2).

Figure 1 shows the XRD patterns of the PLC, BFA, and hardened samples (0C:0A and 5C:0A). The PLC has the expected crystalline phases: alite ($C_3S-Ca_3SiO_5$), belite ($C_2S-Ca_2SiO_4$), calcite ($CaCO_3$) and gypsum ($CaSO_4 \cdot 2H_2O$). This is in agreement with that stated by EN 197:2011 [21] since the PLC used in this work (type II/B-L) is composed of clinker (65 to 79 wt.%) and limestone (21 to 35 wt.%), and with the values expressed in terms of oxides obtained by XRF for CaO (73.06 wt.%) and SiO_2 (12.98 wt.%). The XRD pattern of BFA shows that it is mostly constituted by quartz (SiO_2), calcite ($CaCO_3$), microcline ($KAlSi_3O_8$), sylvite (KCl), calcium hydroxide ($Ca(OH)_2$), and muscovite ($KAl_2(Si_3Al)O_{10}(OH)_2$), thus, in agreement with the main components expressed in terms of oxides detected by XRF (SiO_2 , CaO, K_2O , Al_2O_3 , and Cl). Quartz, calcite and microcline are the crystalline phases commonly found in BFA generated from fluidised bed combustion of forest biomass [2,4,10,11].

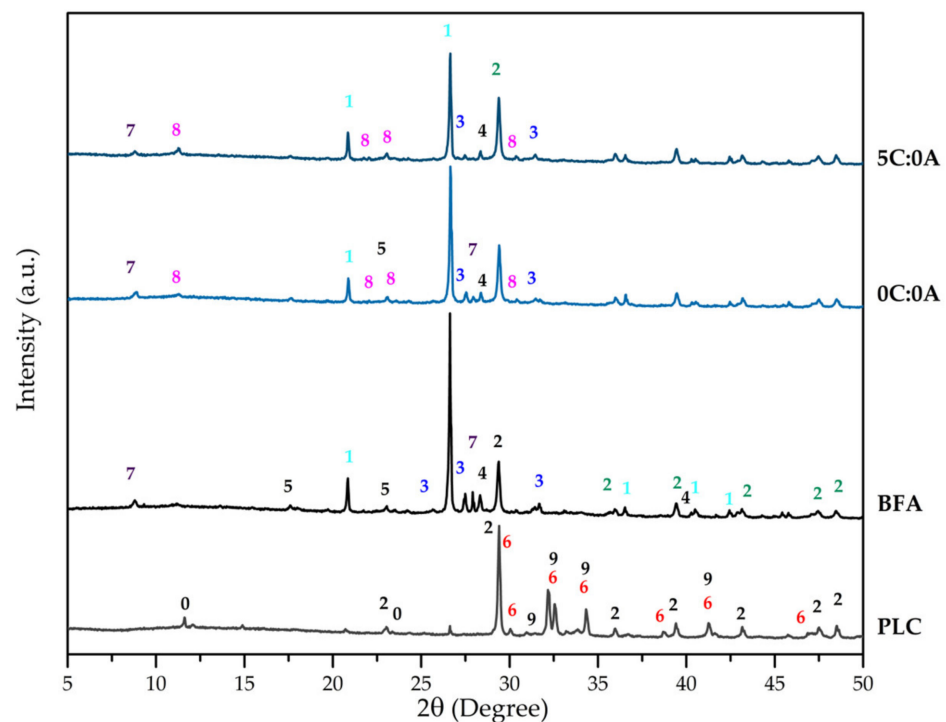


Figure 1. XRD pattern of PLC, BFA and samples 0C:0A and 5C:0A. Numbers stands for: 0- $CaSO_4 \cdot 2H_2O$, 1- SiO_2 , 2- $CaCO_3$, 3- $KAlSi_3O_8$, 4-KCl, 5- $Ca(OH)_2$, 6- Ca_3SiO_5 , 7- $KAl_2(Si_3Al)O_{10}(OH)_2$, 8- $Ca_4Al_2(OH)_{12}(Cl,CO_3,OH)_2 \cdot 4H_2O$, 9- Ca_2SiO_4 .

Figure 2a–d, shows SEM images illustrating the morphology of BFA, PLC and AP, respectively. BFA (Figure 2a,b) and PLC (Figure 2c) are composed of irregularly shaped particles with a broad particle size range, with BFA presenting some acicular-shaped particles. In both materials, it is possible to observe the presence of agglomerates, which are larger in BFA. The particle's size distribution and shape, and the presence of large agglomerates play an important role in the compactness of the samples. The AP (Figure 2d) has a lamellar shape and a coarser particle size when compared to BFA and PLC.

The particle size distribution of BFA and PLC is shown in Figure 3a and 3b, respectively. PLC has a narrower particle size range than BFA and the particles are smaller, in line with SEM observations (Figure 2). BFA has an average particle size of $30.91 \mu m$ and $D_{50} = 19.05 \mu m$, while the PLC has an average particle size of $13.73 \mu m$ and $D_{50} = 9.20 \mu m$. The specific surface area (SSA) of BFA and PLC is $3.24 m^2/g$ and $1.91 m^2/g$, respectively, a result that was not expected taking into consideration the particle size distribution (Figure 3). The higher irregular surface shape and some porosity of BFA particles might explain its higher SSA. The true density of BFA and PLC was found to be $2.57 g/cm^3$ and $3.01 g/cm^3$, respectively.

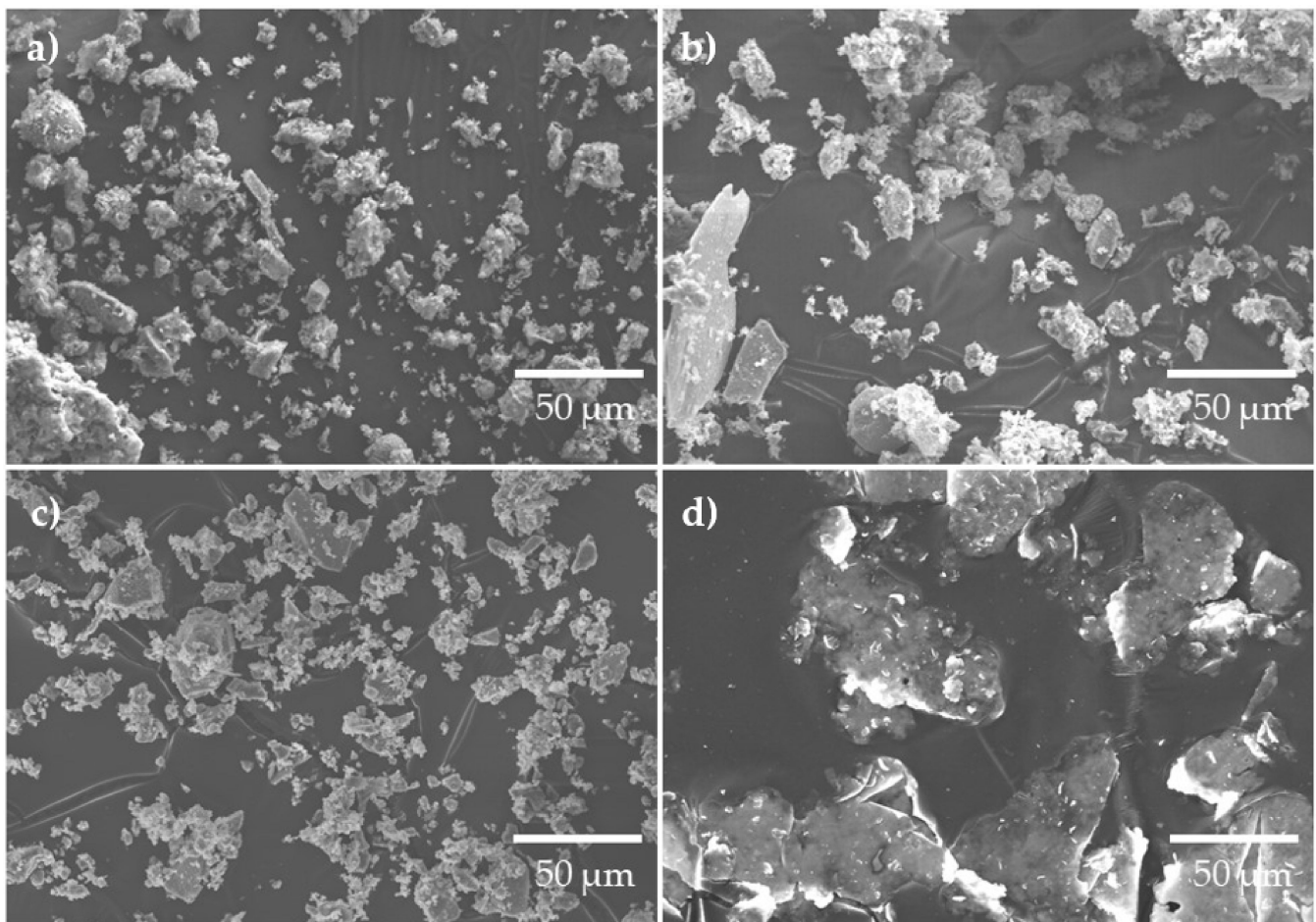


Figure 2. SEM images of BFA (a) and (b), PLC (c) and AP (d).

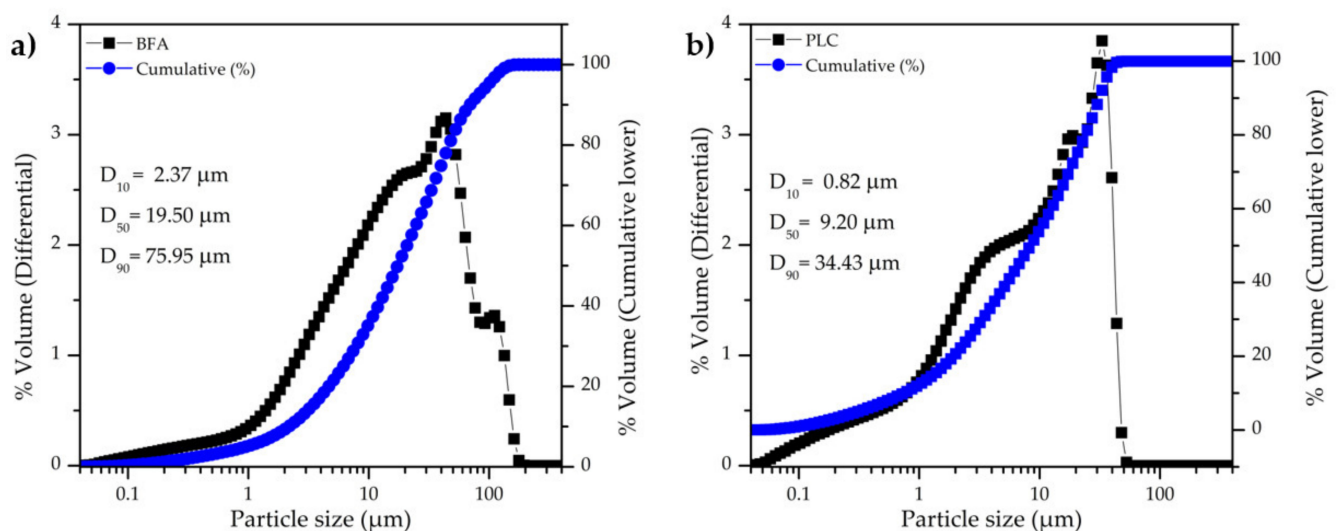


Figure 3. Particle size distribution of powder BFA (a) and PLC (b) samples.

3.2. Monoliths Characterization

The monoliths were characterized for mineralogical composition, density, porosity (total and open), compressive strength and microstructure after 14 days of curing.

The crystalline phases that promote self-hardening and mechanical strength development are related to the reaction of water with the initial phases present in BFA and PLC. The XRD patterns of 0C:0A and 5C:0A hardened samples (Figure 1) reveal the pres-

ence of the crystalline phases already detected in BFA and a new phase—hydrocalumite ($\text{Ca}_4\text{Al}_2(\text{OH})_{12}(\text{Cl}, \text{CO}_3, \text{OH})_2 \cdot 4\text{H}_2\text{O}$). When qualitatively comparing the BFA diffractogram with that of the hardened samples (0C:0A and 5C:0A), it is possible to observe that the intensity of the peaks assigned to quartz (1), calcite (2), microcline (3), sylvite (4) and muscovite (7) decrease. In addition, hydrated aluminosilicate or calcium-rich phases could have also been formed but have a low degree of crystallinity or are present with a concentration below the detection limit.

When comparing the diffractograms of the 5C:0A and 0C:0A samples (Figure 1), it is observed that the intensity of the peaks assigned to quartz (1), microcline (3) and sylvite (4) decreased significantly. The muscovite peak (7) disappears and the intensity of the peaks of calcite and hydrocalumite increases. This is due to the reaction of PLC (5 wt.% added) with water, which releases calcium hydroxide ($\text{Ca}(\text{OH})_2$) into the medium, which may have favoured the formation of a higher quantity of hydrocalumite. Calcite was brought to the system by the PLC addition.

Figure 4a presents the influence of PLC and AP content on the density and porosity (total and open) of the cured samples. A photograph of the parallelepiped samples used in the MB adsorption tests is patent in Figure 4b.

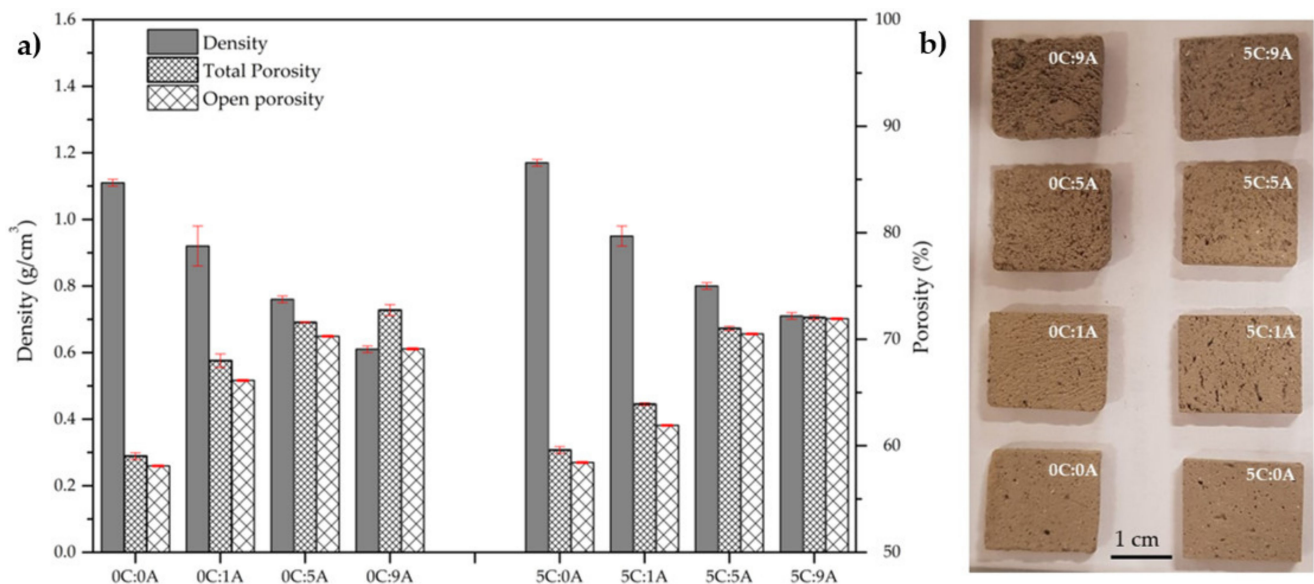


Figure 4. Density and porosity (total and open) of the samples produced with distinct PPLC and AP content (a). Parallelepiped samples used in the MB adsorption tests (b).

The true density (ρ_{th}) of the samples without PLC and AP (0C:0A) and with PLC only (5C:0A) is similar, being 2.63 g/cm^3 and 2.64 g/cm^3 , respectively. The density of the samples decreases as the AP content rises due to the increment of the total porosity. For the samples without PLC, the density varies between 1.11 g/cm^3 (0C:0A sample) and 0.61 g/cm^3 (0C:9A sample). The introduction of 5 wt.% PLC slightly increase the density of the samples (1.17 g/cm^3 for 5C:0A and 0.71 g/cm^3 for 5C:9A). This increment was expected due to PLC characteristics, namely, higher true density, smaller particle size and extended hardening reactions when compared with BFA.

Nevertheless, the samples without AP are already porous ($\approx 58\%$) due to the poor compaction of the BFA particles (presence of acicular-shaped particles and large agglomerates) and the fact that the hydration/hardening reactions of BFA are not intense. As expected, the porosity increases ($\sim 13\%$) with the increment of the porogenic agent. The addition of 0.09 wt.% AP increases the total porosity from 59.0 to 72.7% (samples without PLC) and from 59.6 to 72.0% (samples with 5 wt.% of PLC). For the samples without PLC, the open porosity varies from 58.1 to 69.1% and, for the samples with PLC, it ranges from 58.4 to 71.9%. For all samples, the porosity is almost completely open, which is excellent

for the target application (adsorption of toxic substances). Moreover, the open porosity of the samples, with or without PLC, is similar.

In Figure 4b, it is possible to observe that the macroporosity of the samples increased with AP content. However, the samples without AP also present the same large pores resulting from air entrainment during the mixing process. Interestingly, 0C:9A is the sample that presented the higher difference between the total (72.7%) and the open porosity (69.1%). Macroscopically, looking at Figure 4b, this sample seems to be the one with the largest pores, probably resulting from the coalescence of smaller ones. In sample 5C:9A, this effect is not as evident. Figure 4b also shows that there is anisotropy in the size and the distribution of the pores in all the monoliths.

Figure 5 shows the microstructure of the prepared monoliths, obtained by optical (Figure 5a) and SEM (Figure 5b). In general, it is possible to observe that the porosity increases with the rise of AP content. The addition of PLC (5 wt.%) does not significantly change the mechanism of porosity generation. These observations agree with the values obtained for density and porosity (Figure 4a).

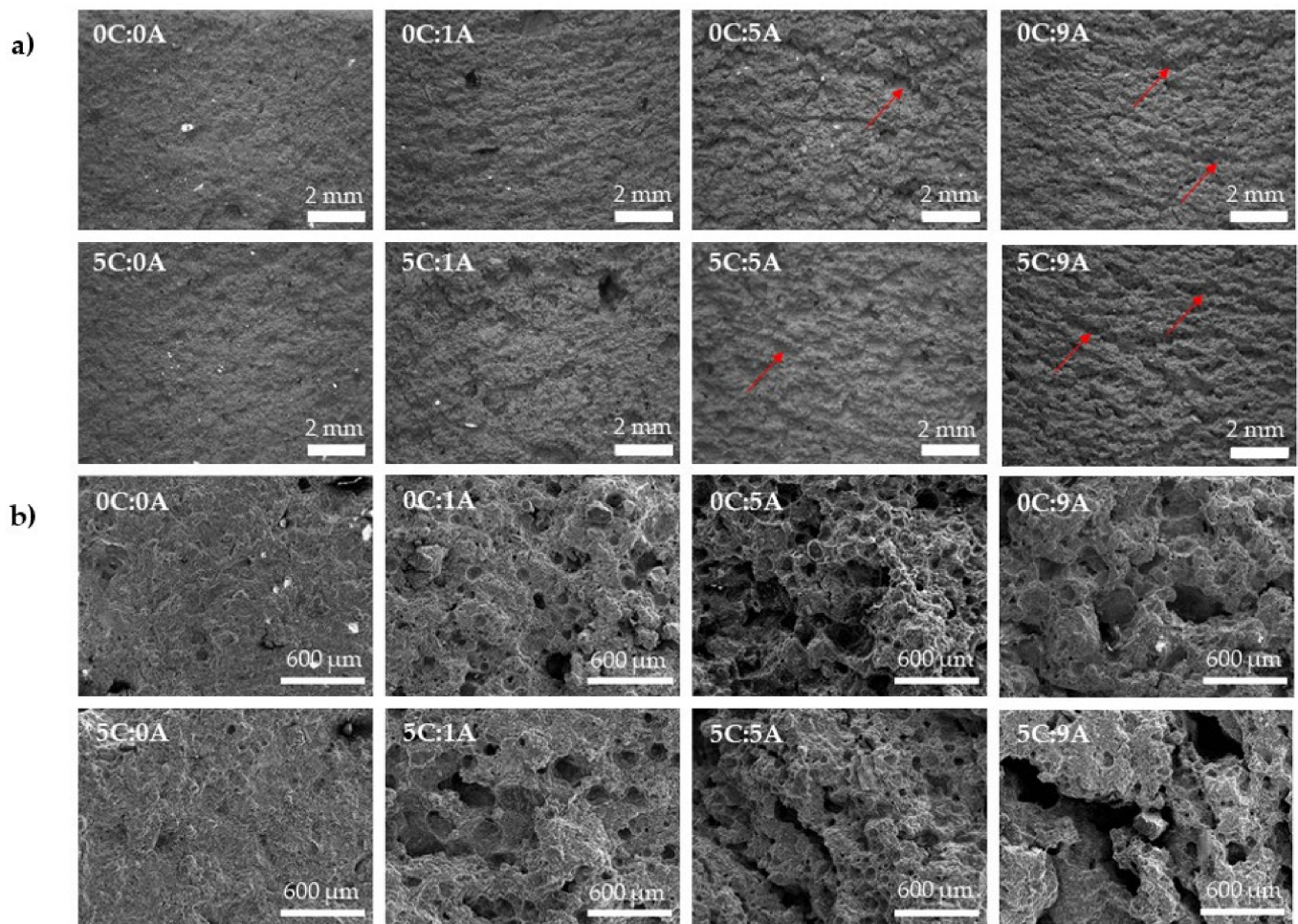


Figure 5. Influence of PLC and AP content on the cured (14 days) monoliths microstructure (a) optical and (b) SEM micrographs. The red arrows indicate examples of the formed macroscopic channels.

In Figure 5a, it is possible to observe, in the samples with AP, the presence of macroscopic channels consisting of interconnected pores. By increasing the AP content (from 0.01 to 0.09 wt.%), the channels tend to be deeper. The released H_2 bubbles Chemical reaction (1) are trapped inside the sample but, during the self-hardening process, they have time to coalesce to some extent, thus generating this type of microstructure. By SEM it is possible to observe the appearance of dispersed rounded pores in the samples with

0.01 wt.% of AP (0C:1A and 5C:1A). This is in line with the decrease in density and the increase in total porosity. However, when the AP content increases from 0.05 to 0.09 wt.%, a decrease in the number of dispersed round pores and the appearance of larger voids resulting from the coalescence/interconnection of smaller pores are observed.

The influence of PLC and AP content on the monoliths' compressive strength is presented in Figure 6a, together with a scheme that exemplifies the PLC effect in the microstructure Figure 6b. The increase in AP content (from 0 to 0.09 wt.%) promotes a decrease in the compressive strength of the samples (from 1.96 to 0.03 MPa in the compositions without PLC) and from 2.70 to 0.23 MPa in the compositions with 5 wt.% of PLC. This behaviour results from the increase in the porosity of the samples. For the same AP amount, the introduction of PLC leads to an increase in the mechanical strength of the samples that results from the better hydraulic characteristics of PLC, in comparison to BFA. PLC promotes stronger bonds between particles and the number of large voids, such as the one seen in Figure 6b, decreased. Such voids tend to exhibit cracks in their inner wall, their occurrence being strongly attenuated by the presence of PLC. This also explains the mechanical resistance improvement in the samples with PLC.

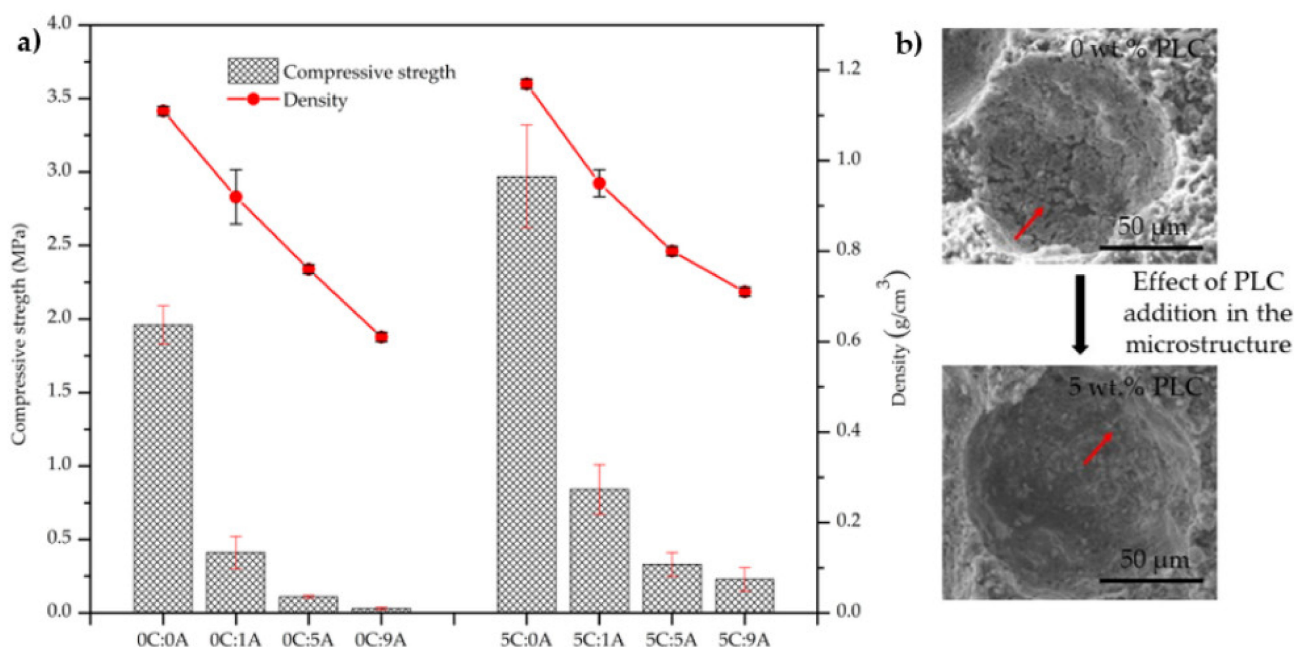


Figure 6. Influence of PLC and AP content on the compressive strength of the monoliths (14 curing days) (a). Detail of the microstructure of cured monoliths without AP and containing or not PLC (b). The red arrows t in evidence the cracks attenuation by the presence of PLC.

The compressive strength of the sample without PLC and AP stays within the range of values reported by Illikainen et al. [5] and Ohenoja et al. [6] for self-hardened monoliths. However, the comparison between the results obtained here and in those works is only indicative since the preparation conditions are very different. In the two mentioned studies, the samples were kept for 28 days at room temperature in closed containers and in this study only 7 days, the water to total solids weight ratio (w/s) was higher (ranging from 0.48 to 1.50) and, although the used fly ash was also from a bubbling fluidised bed boiler, the burned fuel blends are different.

3.3. MB Adsorption Tests

3.3.1. Influence of MB Initial Concentration

The influence of MB initial concentration (1, 2.5, 5, 10 and 15 ppm) on the adsorption of the monoliths after 25 h of contact time was studied. Figure 7 shows the dye uptake (q_e), determined by Equation (4), as a function of initial MB concentration and AP content

in the monoliths. The uptake increases when the MB initial concentration rises, denoting the persistence of available active sites for adsorption (no saturation). Similar behaviour was observed for the AP amount variation since the higher the AP content the higher the uptake values are. This is explained by the increment of the sample's porosity caused by the AP addition. Moreover, the porogenic agent itself can generate active sites within the monoliths that result from the oxidation of the metallic Al ($\text{Al}(\text{OH})_4^-$) Chemical reaction (1). The addition of 5 wt.% of PLC does not significantly affect the uptake values, due to the meaningless microstructural changes obtained by its addition in terms of porosity values (see Figure 4). It should also be noted that some studies [17,22] reported that pure cement shows negligible activity for MB adsorption.

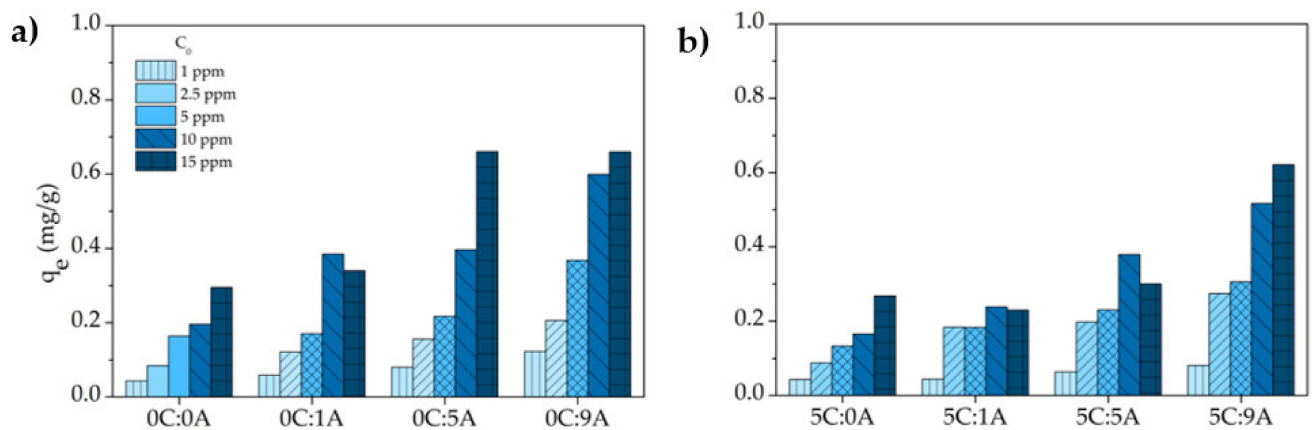


Figure 7. Effect of the initial concentration on the uptake of MB by the different samples (contact time: 25 h): samples prepared without (a) and with PLC (b).

In accordance with the variation of (q_e) with C_0 (Figure 7), the MB removal efficiency (E), determined by Equation (5), increases with the increment of the open porosity of the monoliths and decreases with the rise of the MB concentration (Figure 8). This decrease is due to fact that the number of active sites in each monolith is constant and the higher the MB concentration, the higher the number of molecules of the dye. For example, the increase in the MB concentration from 1 to 15 ppm induces a E reduction of ~53% for the monoliths with the higher AP content with (5C:9A) and without (0C:9A) PLC. For each MB concentration, it is observed that the uptake and the removal efficiency tend to increase with increasing porosity, specifically the open porosity. The existence of more open pores enhances the exposed area of the sample and, consequently, the number of active sites available increases.

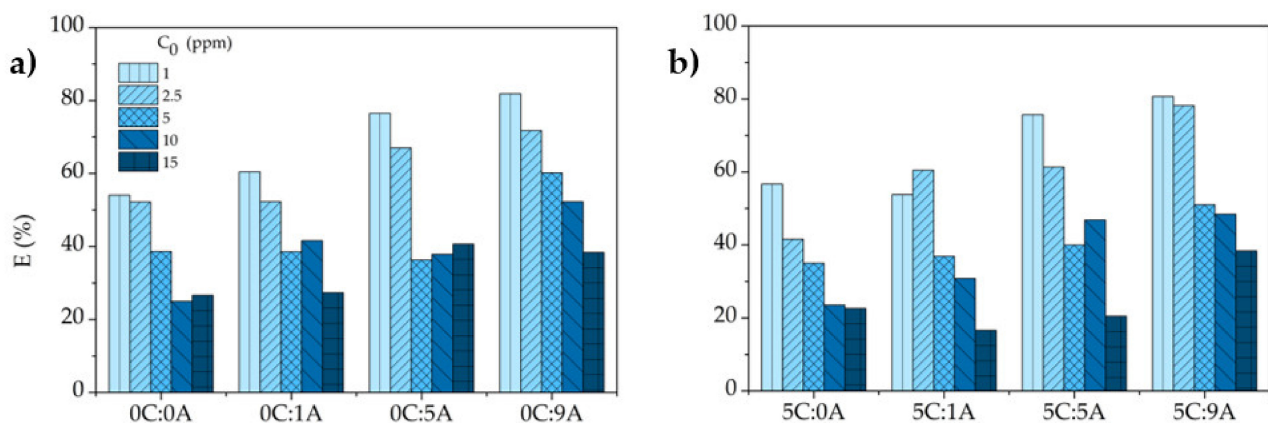


Figure 8. Effect of the initial concentration on the removal efficiency (E) of MB by the different samples (contact time: 25 h): (a) samples without and (b) with PLC.

3.3.2. Influence of Contact Time

Figure 9 shows the effect of contact time (from 0–25 h) on the adsorption performance of the highest porous samples prepared without (0C:9A) and with PLC (5C:9A). As commonly observed, the adsorption is faster in the initial stages (~10 h) and became slower near the equilibrium. However, as higher the concentration of MB, the smaller the absorption rate is in the initial stage because the number of active sites remains constant and there is an increase in the number of dye molecules. The maximum E value was obtained with the lower concentrated MB solution (1 ppm), reaching ~80% for samples without and with PLC.

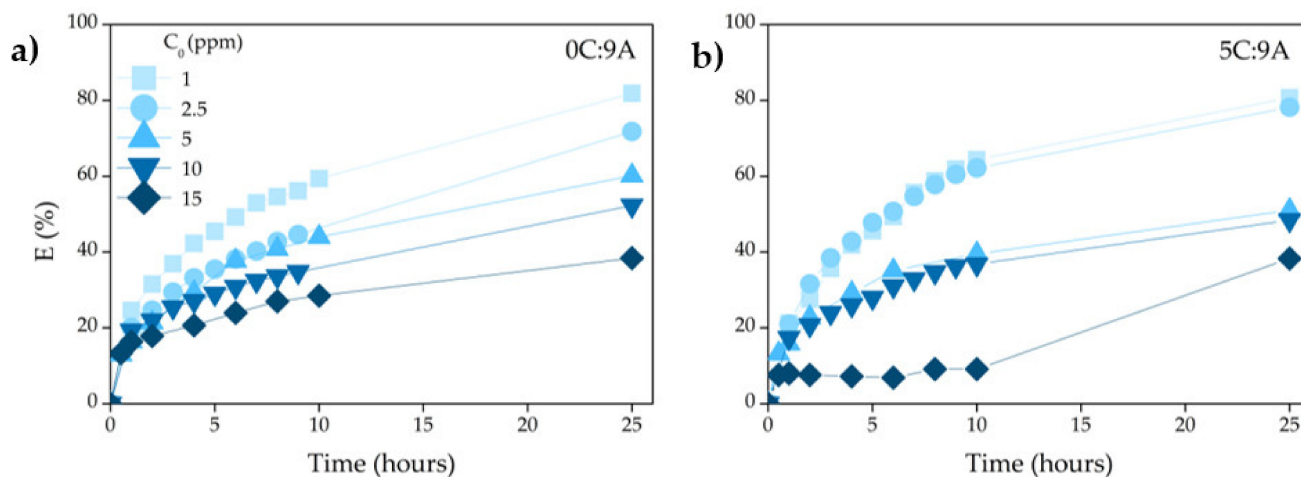


Figure 9. Effect of contact time on the MB adsorption over samples prepared (a) without PLC (0C:9A) and (b) with PLC (5C:9A).

3.3.3. Adsorption Isotherm Model Studies

Experimental data were fitted by the four different linearised forms of the Langmuir isotherms and by the Freundlich isotherms. The better fitting was achieved by the type 2 Langmuir linearisation. The adsorption parameters (q_{max} , K_L) and their corresponding R^2 values are presented in Table 3. After calculating the K_L constant (Equation (7)), the dimensionless separation factor (R_L), which is generally used to express the feasibility of adsorption and affinity between the adsorbent and adsorbate, was determined. For all the samples the R_L values, independently of the initial MB concentration, were between 0 and 1 which means that the adsorption was favourable. The calculated values for q_{max} , which represents the maximum adsorbed capacity in a monolayer, increased with the porosity, from 0.302 to 0.623 mg/g for the samples without PLC, and from 0.219 to 0.657 mg/g for the samples with PLC. For samples with the same Al content, the obtained q_{max} values are very similar, due to the fact that, for the same amount of AP, the total and open porosity values of the samples (with and without PLC) are very similar. As stated above, PLC shows negligible activity for MB adsorption. The calculated values are close to the ones obtained experimentally, Figure 7, meaning that after 25 h the system was close to the equilibrium.

The Freundlich constant K_F and n parameter, and their corresponding linear regression coefficients, were calculated for the different monolith samples analysed, and are shown in Table 4. The R^2 values obtained from the isothermal Langmuir equation were higher than Freundlich's, although all n values are between 1 and 10, which means that the adsorption is favourable.

Thus, the equilibrium data is better characterised by a type 2 Langmuir isotherm model, with a monolayer sorption capacity q_{max} that ranged from 0.219 to 0.657 mg/g. As the use of cement does not significantly alter the adsorption capacity of the monoliths, it should be used only when the experimental layout requires higher mechanical strength.

Table 3. Langmuir adsorption parameters calculated from plotting $1/q_e$ vs. $1/C_e$ for Langmuir linearisation type 2 [14].

	Samples							
	0C:0A	0C:1A	0C:5A	0C:9A	5C:0A	5C:1A	5C:5A	5C:9A
q_{max} (mg/g)	0.302	0.360	0.426	0.623	0.219	0.312	0.371	0.657
K_L (L/mg)	0.351	0.475	0.956	1.305	0.540	0.408	0.965	0.849
R^2	0.991	0.971	0.952	0.989	0.979	0.999	0.989	0.966
R_L								
1 ppm	0.735	0.672	0.504	0.427	0.642	0.704	0.502	0.533
2.5 ppm	0.523	0.448	0.287	0.228	0.416	0.485	0.285	0.312
5 ppm	0.365	0.299	0.174	0.134	0.272	0.331	0.173	0.192
10 ppm	0.235	0.185	0.101	0.076	0.167	0.209	0.101	0.113
15 ppm	0.165	0.127	0.068	0.050	0.114	0.145	0.067	0.075

Table 4. Freundlich adsorption parameters calculated from plotting $\ln q_e$ vs. $\ln C_e$ [14].

	Samples							
	0C:0A	0C:1A	0C:5A	0C:9A	5C:0A	5C:1A	5C:5A	5C:9A
K_F ($\text{mg}^{1-1/n} \text{g}^{-1} \text{L}^{1/n}$)	0.072	0.103	0.161	0.261	0.068	0.080	0.150	0.239
n	1.70	1.71	1.86	2.14	1.87	1.91	2.42	2.16
R^2	0.977	0.930	0.935	0.981	0.982	0.925	0.841	0.887

3.3.4. Adsorption Kinetics Studies

The adsorption kinetic parameters using the pseudo-first-order and pseudo-second-order models were determined to further define the adsorption mechanism of MB for different initial dye concentrations. The results are shown in Table 5. Based on the obtained R^2 and q_e values, the pseudo-first-order model exhibits a better fitting with the experimental data.

Table 5. Kinetic parameters for adsorption of MB onto the samples, initial concentration (C_0), and quantity of adsorbed dye obtained experimentally ($q_e \text{ exp}$).

Samples	C_0 (ppm)	$q_e \text{ exp}$ (mg/g)	Pseudo-First-Order			Pseudo-Second-Order		
			q_e (mg/g)	K_1 (1/min)	R_1^2	q_e (mg/g)	K_2 (g/mg min)	R_2^2
0C:0A	1	0.04	0.034	0.00138	0.996	0.051	0.05027	0.943
	2.5	0.08	0.053	0.00138	0.970	0.094	0.04301	0.964
	5	0.16	0.115	0.00161	0.968	0.176	0.02774	0.963
	10	0.20	0.133	0.00161	0.944	0.220	0.01761	0.969
	15	0.30	0.281	0.00005	0.741	0.975	0.00021	0.042
0C:1A	1	0.06	0.044	0.00161	0.970	0.068	0.04673	0.971
	2.5	0.12	0.092	0.00138	0.997	0.143	0.01865	0.941
	5	0.17	0.130	0.00184	0.996	0.187	0.02396	0.970
	10	0.38	0.292	0.00230	0.990	0.434	0.01046	0.994
	15	0.34	0.304	0.00046	0.671	0.511	0.00125	0.163
0C:5A	1	0.08	0.061	0.00138	0.995	0.093	0.03062	0.954
	2.5	0.16	0.118	0.00161	0.993	0.181	0.01828	0.978
	5	0.22	0.156	0.00230	0.955	0.234	0.02840	0.992
	10	0.40	0.308	0.00230	0.982	0.454	0.00901	0.996
	15	0.66	0.615	0.00115	0.966	1.123	0.00079	0.619
0C:9A	1	0.12	0.091	0.00161	0.992	0.140	0.02451	0.976
	2.5	0.21	0.157	0.00138	0.994	0.245	0.01057	0.943
	5	0.37	0.298	0.00184	0.990	0.413	0.00976	0.977
	10	0.60	0.400	0.00138	0.993	0.674	0.00543	0.960
	15	0.66	0.435	0.00161	0.992	0.702	0.00814	0.971

Table 5. Cont.

Samples	C_0 (ppm)	q_e exp (mg/g)	Pseudo-First-Order			Pseudo-Second-Order		
			q_e (mg/g)	K_1 (1/min)	R_1^2	q_e (mg/g)	K_2 (g/mg min)	R_2^2
5C:0A	1	0.04	0.033	0.00161	0.978	0.051	0.06191	0.975
	2.5	0.09	0.066	0.00161	0.977	0.100	0.03267	0.954
	5	0.13	0.100	0.00138	0.975	0.147	0.02479	0.928
	10	0.17	0.129	0.00138	0.992	0.198	0.01302	0.948
	15	0.27	0.236	0.00014	0.106	0.515	0.00042	0.005
5C:1A	1	0.04	0.043	0.00161	0.995	0.064	0.02164	0.947
	2.5	0.18	0.148	0.00161	0.995	0.215	0.01435	0.968
	5	0.18	0.137	0.00161	0.983	0.201	0.02187	0.957
	10	0.24	0.185	0.00161	0.986	0.282	0.00987	0.959
	15	0.23	0.164	0.00046	0.577	0.272	0.00378	0.188
5C:5A	1	0.06	0.055	0.00207	0.999	0.077	0.03462	0.989
	2.5	0.20	0.156	0.00161	0.994	0.230	0.01324	0.959
	5	0.23	0.171	0.00161	0.960	0.252	0.01745	0.962
	10	0.38	0.312	0.00138	0.997	0.470	0.00464	0.939
	15	0.30	0.257	0.00023	0.321	2.429	0.00003	0.002
5C:9A	1	0.08	0.070	0.00253	0.997	0.096	0.03551	0.993
	2.5	0.27	0.221	0.00230	0.996	0.311	0.01391	0.992
	5	0.31	0.228	0.00207	0.975	0.338	0.02200	0.915
	10	0.52	0.377	0.00184	0.997	0.584	0.00709	0.984
	15	0.62	0.504	0.00007	0.354	0.768	0.00116	0.236

3.3.5. Comparison with Other Studies

Table 6 compares the obtained q_{max} values with several ones reported in the literature for coal fly ash (CFA) and BFA. Most studies used powdered samples and q_{max} values varied between ~ 1 and ~ 11 mg/g, with the minimum value corresponding to trials with NaOH hydrothermally treated CFA. Powdered adsorbents have a much higher concentration of active sites, when compared to porous monoliths, due to their much higher surface area. However, once exhausted, the removal from the aqueous solutions of monoliths is much easier and practical unless the powder is inserted into a container. The q_{max} value (0.62 mg/g) obtained in this study is smaller than the one achieved with BFA-based geopolymer cylindrical monoliths (2.40 mg/g), which can be explained by the higher and more connected porosity in the latter. However, the processing of the monoliths developed in the present work is more sustainable and cheaper since it only uses BFA, water and a very small amount of Al powder. On the contrary, in the production of the geopolymeric samples, metakaolin was added to BFA, and hardening requires the use of alkaline activators (NaOH and sodium silicate), penalizing the cost and the environmental footprint.

Table 6. MB adsorption capacity (q_{max}) of various fly ash adsorbents.

Material	Adsorbent Shape	q_{max} (mg/g)	Ref.
CFA NaOH hydrothermally treated	Powder	10.82	[23]
BFA H ₂ O ₂ heat-treated and sieved	Powder	6.46	[3,24]
CFA grounded	Powder	6.04	[3,13]
CFA washed	Powder	5.72	[16]
CFA unmodified	Powder	2.97	[25]
CFA unmodified	Powder	2.88	[18]
CFA microwave heated in HCl solution	Powder	2.78	[25]
CFA sonicated in HCl solution	Powder	2.58	[25]
BFA-based geopolymer	Cylindrical monolith	2.40 ¹	[4]
CFA ground and sieved	Powder (<90 μ m)	1.47	[3,13]
CFA	powder	1.11	[3,23]
CFA based geopolymer	powder	0.67	[2,26]
BFA based self-hardened	Parallelepiped monolith	0.62	This work

¹ Value obtained for the sample with the higher BFA content before regeneration steps.

Finally, considering the further environmental management of the exhausted monoliths containing MB, they contain a known (but small) dye concentration and can be incorporated in mortar or concrete formulations, acting as light aggregate. If properly managed, dye molecules will remain immobilised in the new matrix and a solution with decreased waste generation might be achieved. In the literature, several works report the valorisation of BFA in cement-based mortars [27–29], as filler or aggregate. Nevertheless, this topic of environmental management of the monoliths produced will be addressed in future work.

4. Conclusions

Biomass fly ash (BFA) has been characterised, converted into an inexpensive porous adsorbent material, and investigated for the removal of methylene blue (MB) from aqueous solutions. The results showed that porous monoliths, with interconnected pores and good mechanical strength, can be used as a low-cost adsorbent for MB removal. Their adsorption capacity increases with the sample porosity and it is possible to produce porous adsorbents with complex geometries without decreasing the adsorption capacity. Furthermore, the use of 5 wt.% Portland limestone cement (PLC) increased the sample's compression strength not interfering with the adsorption process. The adsorption kinetics are in accordance with the pseudo-first-order model and, using the Langmuir isotherms, the maximum adsorptive capacity (q_{\max}) of MB was ≈ 0.6 mg/g having been observed for the highly porous sample (0C:9A and 5C:9A).

These low-cost and environmentally friendly BFA-based adsorbents show promising results for their use in continuous flow systems for MB removal from industrial wastewaters.

Author Contributions: Conceptualization, M.P.S. and J.A.L.; methodology, M.N.C., M.P.S. and J.A.L.; validation, M.N.C., F.R.C., P.C.P., L.A.C.T., M.P.S. and J.A.L.; investigation, M.N.C., F.R.C. and M.P.S.; resources, M.P.S. and J.A.L.; data curation, M.N.C. and F.R.C.; writing—original draft preparation, M.N.C.; writing—review and editing, M.N.C., F.R.C., P.C.P., L.A.C.T., M.P.S. and J.A.L.; supervision, M.P.S.; project administration, P.C.P., L.A.C.T., M.P.S. and J.A.L.; funding acquisition, L.A.C.T., M.P.S. and J.A.L. All authors have read and agreed to the published version of the manuscript.

Funding: This work was supported by Portugal 2020 through the European Regional Development Fund (in the frame of Operational Competitiveness and Internationalization Program) in the scope of the project INPACTUS, POCI/01/0247/FEDER/21874 and in the scope of the project CICECO-Aveiro Institute of Materials, UIDB/50011/2020, UIDP/50011/2020 and LA/P/0006/2020 financed by national funds through the FCT/MEC (PIDDAC). It is acknowledged the financial support to CESAM by the Portuguese Foundation for Science and Technology (FCT)/Ministry of Science, Technology and Higher Education (MCTES) UIDP/50017/2020+UIDB/50017/2020+LA/P/0094/2020, through national funds.

Institutional Review Board Statement: Not applicable.

Informed Consent Statement: Not applicable.

Data Availability Statement: Not applicable.

Conflicts of Interest: The authors declare no conflict of interest.

References

1. Leflaivei, X.; Witmer, M.; Martin-Hurtado, R.; Bakker, M.; Kram, T.; Bouwman, L.; Visser, H.; Bouwman, A.; Hilderink, H.; Kayoung, K. "Water" in *OECD Environmental Outlook to 2050: The Consequences of Inaction*; OECD Publishing: Paris, France, 2012. [[CrossRef](#)]
2. Novais, R.M.; Carvalheiras, J.; Tobaldi, D.M.; Seabra, M.P.; Pullar, R.C.; Labrincha, J.A. Synthesis of porous biomass fly ash-based geopolymer spheres for efficient removal of methylene blue from wastewaters. *J. Clean. Prod.* **2019**, *207*, 350–362. [[CrossRef](#)]
3. Rafatullah, M.; Sulaiman, O.; Hashim, R.; Ahmad, A. Adsorption of methylene blue on low-cost adsorbents: A review. *J. Hazard. Mater.* **2010**, *177*, 70–80. [[CrossRef](#)] [[PubMed](#)]
4. Novais, R.M.; Ascensão, G.; Tobaldi, D.M.; Seabra, M.P.; Labrincha, J.A. Biomass fly ash geopolymer monoliths for effective methylene blue removal from wastewaters. *J. Clean. Prod.* **2018**, *171*, 783–794. [[CrossRef](#)]

5. Illikainen, M.; Tanskanen, P.; Kinnunen, P.; Körkkö, M.; Peltosaari, O.; Wigren, V.; Österbacka, J.; Talling, B.; Niinimäki, J. Reactivity and self-hardening of fly ash from the fluidized bed combustion of wood and peat. *Fuel* **2014**, *135*, 69–75. [[CrossRef](#)]
6. Ohenoja, K.; Tanskanen, P.; Wigren, V.; Kinnunen, P.; Körkkö, M.; Peltosaari, O.; Österbacka, J.; Illikainen, M. Self-hardening of fly ashes from a bubbling fluidized bed combustion of peat, forest industry residuals, and wastes. *Fuel* **2016**, *165*, 440–446. [[CrossRef](#)]
7. Ohenoja, K.; Tanskanen, P.; Peltosaari, O.; Wigren, V.; Österbacka, J.; Illikainen, M. Effect of particle size distribution on the self-hardening property of biomass-peat fly ash from a bubbling fluidized bed combustion. *Fuel Process. Technol.* **2016**, *148*, 60–66. [[CrossRef](#)]
8. Sigvardsen, N.M.; Geiker, M.R.; Ottosen, L.M. Reaction mechanisms of wood ash for use as a partial cement replacement. *Constr. Build. Mater.* **2021**, *286*, 122889. [[CrossRef](#)]
9. European Commission. A Roadmap for Moving to a Competitive Low Carbon Economy in 2050. 2011. Available online: <http://eur-lex.europa.eu/LexUriServ/LexUriServ.do?uri=COM:2011:0112:FIN:EN:PDF> (accessed on 13 April 2021).
10. Tarelho, L.A.C.; Teixeira, E.R.; Silva, D.F.R.; Modolo, R.C.E.; Labrincha, J.A.; Rocha, F. Characteristics of distinct ash flows in a biomass thermal power plant with bubbling fluidised bed combustor. *Energy* **2015**, *90*, 387–402. [[CrossRef](#)]
11. Novais, R.M.; Ascensão, G.; Ferreira, N.; Seabra, M.P.; Labrincha, J.A. Influence of water and aluminium powder content on the properties of waste-containing geopolymer foams. *Ceram. Int.* **2018**, *44*, 6242–6249. [[CrossRef](#)]
12. Hertel, T.; Novais, R.M.; Alarcón, R.M.; Labrincha, J.A.; Pontikes, Y. Use of modified bauxite residue-based porous inorganic polymer monoliths as adsorbents of methylene blue. *J. Clean. Prod.* **2019**, *227*, 877–889. [[CrossRef](#)]
13. Janoš, P.; Buchtová, H.; Rýznarová, M. Sorption of dyes from aqueous solutions onto fly ash. *Water Res.* **2003**, *37*, 4938–4944. [[CrossRef](#)] [[PubMed](#)]
14. Kumar, K.V.; Sivanesan, S. Isotherms for Malachite Green onto rubber wood (*Hevea brasiliensis*) sawdust: Comparison of linear and non-linear methods. *Dye. Pigment.* **2007**, *72*, 124–129. [[CrossRef](#)]
15. Ayawei, N.; Ebelegi, A.N.; Wankasi, D. Modelling and Interpretation of Adsorption Isotherms. *J. Chem.* **2017**, *2017*, 3039817. [[CrossRef](#)]
16. Kumar, K.V.; Ramamurthi, V.; Sivanesan, S. Modeling the mechanism involved during the sorption of methylene blue onto fly ash. *J. Colloid Interface Sci.* **2005**, *284*, 14–21. [[CrossRef](#)] [[PubMed](#)]
17. Singh, V.P.; Vaish, R. Cement-based diesel exhaust emission soot coatings for the removal of organic pollutants from water. *Constr. Build. Mater.* **2020**, *234*, 117377. [[CrossRef](#)]
18. El Alouani, M.; Alehyen, S.; el Achouri, M.; Taibi, M. Comparative study of the adsorption of micropollutant contained in aqueous phase using coal fly ash and activated coal fly ash: Kinetic and isotherm studies. *Chem. Data Collect.* **2019**, *23*, 100265. [[CrossRef](#)]
19. Rajamma, R.; Senff, L.; Ribeiro, M.J.; Labrincha, J.A.; Ball, R.J.; Allen, G.C.; Ferreira, V.M. Biomass fly ash effect on fresh and hardened state properties of cement based materials. *Compos. Part B Eng.* **2015**, *77*, 1–9. [[CrossRef](#)]
20. Ohenoja, K.; Pesonen, J.; Yliniemi, J.; Illikainen, M. Utilization of fly ashes from fluidized bed combustion: A review. *Sustainability* **2020**, *12*, 2988. [[CrossRef](#)]
21. EN 197-1:2011; Cement Part 1: Composition, Specifications and Conformity Criteria for Common Cements. CEN: Brussels, Belgium, 2011.
22. Huang, J.; Koroteev, D.D.; Zhang, M. Smartphone-based study of cement-activated charcoal coatings for removal of organic pollutants from water. *Constr. Build. Mater.* **2021**, *300*, 124034. [[CrossRef](#)]
23. Woolard, C.D.; Strong, J.; Erasmus, C.R. Evaluation of the use of modified coal ash as a potential sorbent for organic waste streams. *Appl. Geochem.* **2002**, *17*, 1159–1164. [[CrossRef](#)]
24. Gupta, V.K.; Mohan, D.; Sharma, S.; Sharma, M. Removal of basic dyes (rhodamine B and methylene blue) from aqueous solutions using bagasse fly ash. *Sep. Sci. Technol.* **2000**, *35*, 2097–2113. [[CrossRef](#)]
25. Wang, S.; Boyjoo, Y.; Choueib, A. A comparative study of dye removal using fly ash treated by different methods. *Chemosphere* **2005**, *60*, 1401–1407. [[CrossRef](#)] [[PubMed](#)]
26. Zhang, Y.; Liu, L. Fly ash-based geopolymer as a novel photocatalyst for degradation of dye from wastewater. *Particuology* **2013**, *11*, 353–358. [[CrossRef](#)]
27. Berra, M.; Mangialardi, T.; Paolini, A.E. Reuse of woody biomass fly ash in cement-based materials. *Constr. Build. Mater.* **2015**, *76*, 286–296. [[CrossRef](#)]
28. Cuenca, J.; Rodríguez, J.; Martín-Morales, M.; Sánchez-Roldán, Z.; Zamorano, M. Effects of olive residue biomass fly ash as filler in self-compacting concrete. *Constr. Build. Mater.* **2013**, *40*, 702–709. [[CrossRef](#)]
29. Modolo, R.C.E.; Senff, L.; Ferreira, V.M.; Tarelho, L.A.C.; Moraes, C.A.M. Fly ash from biomass combustion as replacement raw material and its influence on the mortars durability. *J. Mater. Cycles Waste Manag.* **2018**, *20*, 1006–1015. [[CrossRef](#)]